Characteristics of GPS, BDS2, BDS3 and Galileo inter-system biases and their influence on RTK positioning

Xiaolong Mi[1, 2], Baocheng Zhang[1], Yunbin Yuan[1], Xiaowen Luo[3]

Baocheng Zhang (✉)

Email: b.zhang@whigg.ac.cn

1. State Key Laboratory of Geodesy and Earth's Dynamics, Institute of Geodesy and Geophysics, Wuhan, China

2. University of Chinese Academy of Sciences, Beijing, China

3. The Second Institute of Oceanography, SOA, Hangzhou, 310012, China

IOP Publishing Measurement Science and Technology
Meas. Sci. Technol. 31 (2020) 015009 (12pp) https://doi.org/10.1088/1361-6501/ab4209

Characteristics of GPS, BDS2, BDS3 and Galileo inter-system biases and their influence on RTK positioning

Xiaolong Mi[1,2], Baocheng Zhang[1,4], Yunbin Yuan[1] and Xiaowen Luo[3]

[1] State Key Laboratory of Geodesy and Earth's Dynamics, Institute of Geodesy and Geophysics, Wuhan, People's Republic of China
[2] University of Chinese Academy of Sciences, Beijing, People's Republic of China
[3] The Second Institute of Oceanography, SOA, Hangzhou, 310012, People's Republic of China

E-mail: b.zhang@whigg.ac.cn

Received 9 June 2019, revised 26 August 2019
Accepted for publication 6 September 2019
Published 24 October 2019

Abstract

The Chinese new-generation BeiDou navigation satellite system (BDS3) is under construction and has begun to provide satellite-based positioning, navigation and timing solutions for global users. Inter-system biases (ISBs) are critical for the optimal combination of multiple global navigation satellite systems (GNSSs) observations, and their calibration makes it possible to enhance the interoperability among different GNSSs. We formerly presented a method based on the between-receiver single-differenced (SD) multi-GNSS observation equations for estimating the ISBs in scenarios with both overlapping and non-overlapping frequencies. In this paper, we analyze the ISBs between the new-generation BDS3 and other GNSSs, as well as BDS2, using the previously proposed SD method. For the first time, this article presents the ISBs between BDS3 and GPS, Galileo and BDS2 for identical-receiver baselines. Numerical analysis indicates that (1) the new frequencies of BDS3 that overlap those of GPS and Galileo are, rather unexpectedly, free of ISBs, suggesting the existence of interoperability among these three constellations; (2) there are obvious ISBs between BDS3 and BDS2 at non-overlapping frequencies but not at overlapping frequencies; (3) calibrating the ISBs makes it possible to improve the performance of real-time kinematic (RTK) positioning for multiple GNSSs involving BDS3.

Keywords: new-generation BeiDou navigation satellite system (BDS3), global navigation satellite systems (GNSSs), inter-system biases (ISBs), ionospheric-fixed model

(Some figures may appear in colour only in the online journal)

Introduction

Since China began to independently build the BeiDou navigation satellite system (BDS), a 'three-step' strategy has clearly been followed (Zhang *et al* 2017, Li *et al* 2019). The first step was the development of the BeiDou navigation satellite demonstration system (BDS1), after which China committed to establishing the regional system serving the Asia-Pacific region, known as BDS2 (Yang *et al* 2014). BDS2 is a constellation of 15 satellites, including five satellites in geostationary orbit (GEO), seven in inclined geosynchronous orbit (IGSO) and three in medium-altitude Earth orbit (MEO). BDS2 satellites transmit navigation signals at three frequencies, namely, B1I at 1561.098 MHz, B2I at 1207.140 MHz and B3I at 1268.520 MHz (Yang *et al* 2018, Cao *et al* 2019). BDS3 is the third and most important step in the globalization of BDS, the goal of which is to build a full constellation consisting of 35 satellites, including five GEO, 27 MEO and three IGSO satellites by 2020; such a constellation would provide reliable positioning, navigation and timing (PNT) services for global users (Yang *et al* 2019). To achieve compatibility and interoperability

[4] Author to whom any correspondence should be addressed.

with other global navigation satellite systems (GNSSs), BDS3 transmits several new navigational signals in space, including B1C at 1575.42 MHz and B2a at 1176.450 MHz, which overlap with L1 and L5 of GPS and E1 and E5a of Galileo (Zhao *et al* 2017). Fortunately, on December 27, 2018, China officially announced that BDS3 has the capability to provide basic services for global users, which prompted us to conduct scientific research focused on BDS3 (Wang *et al* 2019).

However, to maximize the benefit of the combined processing of data from different GNSSs, we must address some key issues related to interoperability at the signal level (Gao *et al* 2019, Liu *et al* 2019). In addition to the unification of coordinates and time reference frames that tend to differ across GNSS constellations, the inter-system biases (ISBs) should also be considered (El-Mowafy *et al* 2016, Gao *et al* 2017). ISBs are caused by the correlation process of the GNSS receiver and occur in both the carrier phase and code data (Odijk and Teunissen 2012, Gioia and Borio 2016, Odijk *et al* 2016). Several investigations of ISBs have been conducted, typically using a double-differenced (DD) model to focus on overlapping frequencies (Nadarajah *et al* 2014, Paziewski and Wielgosz 2014, Paziewski *et al* 2015). Because the frequencies of any two GNSS constellations may not overlap completely, we proposed a method based on a single-differenced (SD) model that is applicable for the estimation of ISBs for both overlapping and non-overlapping frequencies in a previous study (Mi *et al* 2019b).

In this contribution, we present an investigation of the ISBs between BDS3 and GPS, BDS3 and Galileo and BDS3 and BDS2 for the first time. Using the new-generation Trimble Alloy, which can track the signals of BDS3, one zero baseline and one short baseline are created, and 10 d of multi-GNSS data are collected. The code and phase ISBs for the new BDS3 frequencies that are shared with GPS and Galileo are analyzed in detail. In addition, the ISBs of overlapping and non-overlapping frequencies between BDS3 and BDS2 are studied. Finally, the real-time kinematic (RTK) positioning performance with ISBs calibrated based on multiple GNSSs involving BDS3 is discussed.

In this paper, the ISBs estimation model and its applications based on the between-receiver SD are reviewed. Then, the GNSS data collection process and the experimental results for ISBs estimation in different applications based on real BDS (both BDS2 and BDS3), GPS and Galileo data are summarized and analyzed.

RTK model: ISBs estimation and applications

Consider a zero- or short-baseline configuration for which one can safely assume no differential ionospheric or tropospheric effects (Odolinski *et al* 2014c, Zhang *et al* 2016, Mi *et al* 2019a). The rank-deficient RTK model using an SD code and phase observations of dual constellations can be given as

$$\begin{aligned} p_{j_A}^{s_A} &= g^{s_A^T} x_{\mathrm{r}} + \mathrm{d}t + d_{j_A}^A \\ \phi_{j_A}^{s_A} &= g^{s_A^T} x_{\mathrm{r}} + \mathrm{d}t + \delta_{j_A}^A + \lambda_{j_A} z_{j_A}^{s_A} \\ p_{j_B}^{s_B} &= g^{s_B^T} x_{\mathrm{r}} + \mathrm{d}t + d_{j_B}^B \\ \phi_{j_B}^{s_B} &= g^{s_B^T} x_{\mathrm{r}} + \mathrm{d}t + \delta_{j_B}^B + \lambda_{j_B} z_{j_B}^{s_B} \end{aligned} \tag{1}$$

where A and B denote different GNSS constellations and we use the symbol $*$ to represent them. $p_{j_*}^{s_*}$ and $\phi_{j_*}^{s_*}$ denote the vectors of the SD code and the phase observables of satellite s_* at frequency j_* for a GNSS constellation, for which the approximate geometric range and tropospheric delay have been previously corrected. The symbol x_{r} denotes a column vector of geometric unknowns consisting of three baselines, and the corresponding coefficient g^{s_*} is a row vector of the receiver-to-satellite unit vector. The symbols $\lambda_{j_*}^*$ and $z_{j_*}^{s_*}$ indicate the wavelength and SD ambiguity. The receiver-dependent unknown parameters can be classified as the receiver clock $\mathrm{d}t$, receiver code bias $d_{j_*}^*$ and receiver phase bias $\delta_{j_*}^*$. Note that, when creating SD observations, the satellite-specific errors including time offset between different GNSSs are eliminated.

However, the SD observation equations are not full rank and should be eliminated through an application of S-system theory (Odolinski *et al* 2013, 2014a). The rank deficiency for equation (1) comes from two sources: the rank defects between the receiver clock and code/phase delays and those between the phase delays and ambiguities (Odolinski *et al* 2014b). It is common practice to eliminate these rank deficiencies by selecting the S-basis for each constellation, which can be regarded as classical differencing (Deng *et al* 2014, Odolinski *et al* 2015). However, this approach does not fully exploit the advantages of using multi-GNSS signals (Jiang *et al* 2017). Alternatively, instead of applying this classical differencing approach, we can select unknown parameters for only one constellation as the S-basis to eliminate the rank deficiencies. This approach can be characterized as inter-system differencing, which fully exploits the advantages of multi-GNSS signals (Li *et al* 2017, Mi *et al* 2019b). In this paper, the basis of the full-rank RTK model is inter-system differencing, and hence, ISBs can be naturally introduced.

Once the rank deficiency problems above have been solved, the dual-GNSS RTK model can be formulated in the following full-rank linearized SD system of observations, which can be expressed as

$$\begin{aligned} p_{j_A}^{s_A} &= g^{s_A^T} x_{\mathrm{r}} + \mathrm{d}\tilde{t} + \tilde{d}_{j_A}^A \\ \phi_{j_A}^{s_A} &= g^{s_A^T} x_{\mathrm{r}} + \mathrm{d}\tilde{t} + \tilde{\delta}_{j_A}^A + \lambda_{j_A} \tilde{z}_{j_A}^{1s_A} \\ p_{j_B}^{s_B} &= g^{s_B^T} x_{\mathrm{r}} + \mathrm{d}\tilde{t} + \tilde{d}_{j_B}^B \\ \phi_{j_B}^{s_B} &= g^{s_B^T} x_{\mathrm{r}} + \mathrm{d}\tilde{t} + \tilde{\delta}_{j_B}^B + \lambda_{j_B} \tilde{z}_{j_B}^{1s_B} \end{aligned} \tag{2}$$

where some parameters are given new meanings after reorganization. The specific meanings are given in table 1.

Because (2) represents a full-rank system, the code or phase ISBs can be obtained by differencing the SD code or phase observations between the two constellations, and this process can be expressed as

$$\begin{aligned} \tilde{\tilde{p}}_{j_{AB}}^{s_{AB}} &= (g^{s_B^T} - g^{s_A^T}) x_{\mathrm{r}} + \tilde{\tilde{d}}_{j_{AB}}^{AB} \\ \tilde{\tilde{\phi}}_{j_{AB}}^{s_{AB}} &= (g^{s_B^T} - g^{s_A^T}) x_{\mathrm{r}} + \tilde{\tilde{\delta}}_{j_B}^A + \lambda_{j_{AB}} z_{j_{AB}}^{1s_{AB}} \end{aligned} \tag{3}$$

where $\tilde{\tilde{p}}_{j_{AB}}^{s_{AB}} = p_{j_B}^{s_B} - p_{j_A}^{s_A}$, $\tilde{\tilde{\phi}}_{j_{AB}}^{s_{AB}} = \phi_{j_B}^{s_B} - \phi_{j_A}^{s_A}$ and $z_{j_{AB}}^{1s_{AB}} = z_{j_B}^{1s_B} - z_{j_A}^{1s_A}$. In addition, $\tilde{\tilde{d}}_{j_{AB}}^{AB}$ represents code ISBs without any bias, and $\tilde{\tilde{\delta}}_{j_{AB}}^{AB} = \delta_{j_{AB}}^{AB} + \lambda_{j_{AB}} z_{j_{AB}}^{1_{AB}}$ gives the phase ISBs biased by the SD

Table 1. Estimated unknown parameters and their interpretations in the ionospheric-fixed model.

Notation and interpretation	Estimated parameter
$\tilde{\mathrm{d}t} = \mathrm{d}t + d^A_{1_A}$	Receiver clock with the code bias of GNSS A for $j_A = 1$
$\tilde{d}^A_{j_A} = d^A_{j_A} - d^A_{1_A}$	Receiver code bias of GNSS A, where $j_A \geqslant 2$
$\tilde{\delta}^A_{j_A} = \delta^A_{j_A} - d^A_{1_A} + \lambda^A_{j_A} z^{1_A}_{j_A}$	Receiver phase bias of GNSS A, where $j_A \geqslant 1$
$\tilde{d}^B_{j_B} = d^B_{j_B} - d^A_{1_A}$	Receiver code bias of GNSS B, where $j_B \geqslant 1$
$\tilde{\delta}^B_{j_B} = \delta^B_{j_B} - d^A_{1_A} + \lambda^B_{j_B} z^{1_B}_{j_B}$	Receiver phase bias of GNSS B, where $j_B \geqslant 1$
$\tilde{z}^{1s_A}_{j_A} = z^{s_A}_{j_A} - z^{1_A}_{j_A}$ or $\tilde{z}^{1s_B}_{j_B} = z^{s_B}_{j_B} - z^{1_B}_{j_B}$	DD integer ambiguities, where $j_* \geqslant 1$ and $s_* \geqslant 2$

ambiguity of reference satellites. Thus, the ISBs are estimated in two steps.

Based on (3), the first step is to resolve the baseline $(g^{s^T_B} - g^{s^T_A})x_\mathrm{r}$ and the DD ambiguities $\lambda_{j_B} z^{1s_B}_{j_B}$ and $\lambda_{j_A} z^{1s_A}_{j_A}$, which can be precisely determined using the entire observation series. For a zero or short baseline, we consider this task to be very easy. Once $\lambda_{j_B} z^{1s_B}_{j_B}$ and $\lambda_{j_A} z^{1s_A}_{j_A}$ have been resolved, $\lambda_{j_{AB}} z^{1s_{AB}}_{j_{AB}}$can be determined.

The second step is to substitute the baseline and DD ambiguities from $\tilde{\phi}^{s_{AB}}_{j_{AB}}$, which are precisely determined in the first step, yielding

$$\begin{aligned} \bar{p}^{s_{AB}}_{j_{AB}} &= \tilde{\tilde{d}}^{AB}_{j_{AB}} \\ \bar{\phi}^{s_{AB}}_{j_{AB}} &= \tilde{\tilde{\delta}}^{AB}_{j_{AB}} \end{aligned} \tag{4}$$

where $\bar{p}^{s_{AB}}_{j_{AB}} = \tilde{\tilde{p}}^{s_{AB}}_{j_{AB}} - (g^{s^T_B} - g^{s^T_A})x_\mathrm{r}$ and $\bar{p}^{s_{AB}}_{j_{AB}} = \tilde{\tilde{p}}^{s_{AB}}_{j_{AB}} - (g^{s^T_B} - g^{s^T_A})x_\mathrm{r} - \lambda_{j_{AB}} z^{1s_{AB}}_{j_{AB}}$. We conclude this step by solving for $\tilde{\tilde{d}}^{AB}_{j_{AB}}$ and $\tilde{\tilde{\delta}}^{AB}_{j_{AB}}$ using least-square estimation.

Once the ISBs are isolated, the dual-GNSS RTK model can be formulated as follows

$$\begin{aligned} p^{s_A}_{j_A} &= g^{s^T_A} x_\mathrm{r} + \tilde{\mathrm{d}t} + \tilde{\tilde{d}}^A_{j_A} \\ \phi^{s_A}_{j_A} &= g^{s^T_A} x_\mathrm{r} + \tilde{\mathrm{d}t} + \tilde{\tilde{\delta}}^A_{j_A} + \lambda_{j_A} \tilde{z}^{1s_A}_{j_A} \\ p^{s_B}_{j_B} &= g^{s^T_B} x_\mathrm{r} + \tilde{\mathrm{d}t} + \tilde{\tilde{d}}^A_{j_A} + \tilde{\tilde{d}}^{AB}_{j_{AB}} \\ \phi^{s_B}_{j_B} &= g^{s^T_B} x_\mathrm{r} + \tilde{\mathrm{d}t} + \tilde{\tilde{\delta}}^A_{j_A} + \tilde{\tilde{\delta}}^{AB}_{j_{AB}} + \lambda_{j_B} \tilde{z}^{1s_B}_{j_B}. \end{aligned} \tag{5}$$

This equation set is the application model of ISBs in RTK positioning. In this situation, we can use the *a priori* knowledge of the ISBs to correct them from observations or estimate them as time-invariant unknowns, both of which can strengthen the model.

Here, the estimation and application of ISBs are based on zero or short baselines, and because there are no ionospheric effects, the model can be characterized as an ionospheric-fixed model (Odijk and Teunissen 2010). The details of the estimation and application of ISBs using the ionospheric-weighted and ionospheric-float models can be found in previous studies and will not be repeated here (Mi *et al* 2019b).

Table 2. Summary of the antenna types used in the experiment for three receivers (IGG50, IGG51 and IGG52).

Observation period	Antenna type
011-012	Trimble Zephyr 3 (geodetic grade)
013	Trimble Zephyr 3 (geodetic grade)
014-015	South GR3-G3 (geodetic grade)
016	South GR3-G3 (geodetic grade)
017	South GGBR044P00S (surveying grade)
018-020	South GGBR044P00S (surveying grade)

IGG50 and IGG52 share a common antenna whereas IGG51 uses a single antenna; the daily antenna type is the same. With these three receivers, we can form one zero baseline and one short baseline. It is worth noting that IGG51 is close to high-rise buildings and can reflect the advantages of multi-GNSS inter-system differencing.

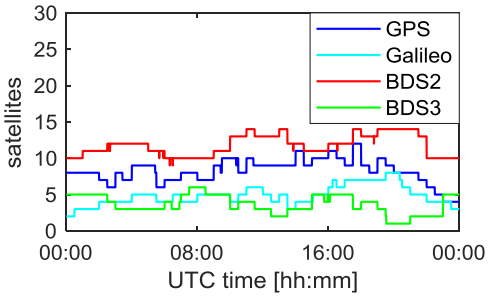

Figure 1. The number of visible GPS, BDS and Galileo satellites for IGG52, with an elevation cut-off of 5°, on January 13, 2019, of which BDS2 and BDS3 are counted separately.

Experiments and results

In this section, we first describe the setup of the experiments, including the experimental environment and the datasets. Then, a summary of the experimental results is given, including the ISBs estimation and RTK positioning results based on the application of ISBs.

Experimental setup

In our analysis, we selected two sets of GNSS data (one zero baseline and one short baseline of 69 m), each measured by two identical Trimble Alloy receivers deployed on the roof of an office building of the Institute of Geodesy and Geophysics, Wuhan (114.4 °E, 30.6 °S). The data were collected over ten consecutive days (DOY 011-020, 2019) with the signals of three constellations, including the new-generation BDS3, and a 30 s interval. The data from the first and last two hours (UTC 0-2, 22-24) were not used because we either replaced the antenna or changed the configuration of the receiver at those times. In addition, three different types of antennas (the surveying-grade South GGBR044P00S antenna, geodetic-grade South GR3-G3 and Trimble Zephyr3 antennas) were connected for different observation periods. For more details regarding the antenna type, see table 2. The data acquired over six days were selected for ISBs estimation, and the data recorded on two days were selected to validate the effect of ISBs on RTK positioning.

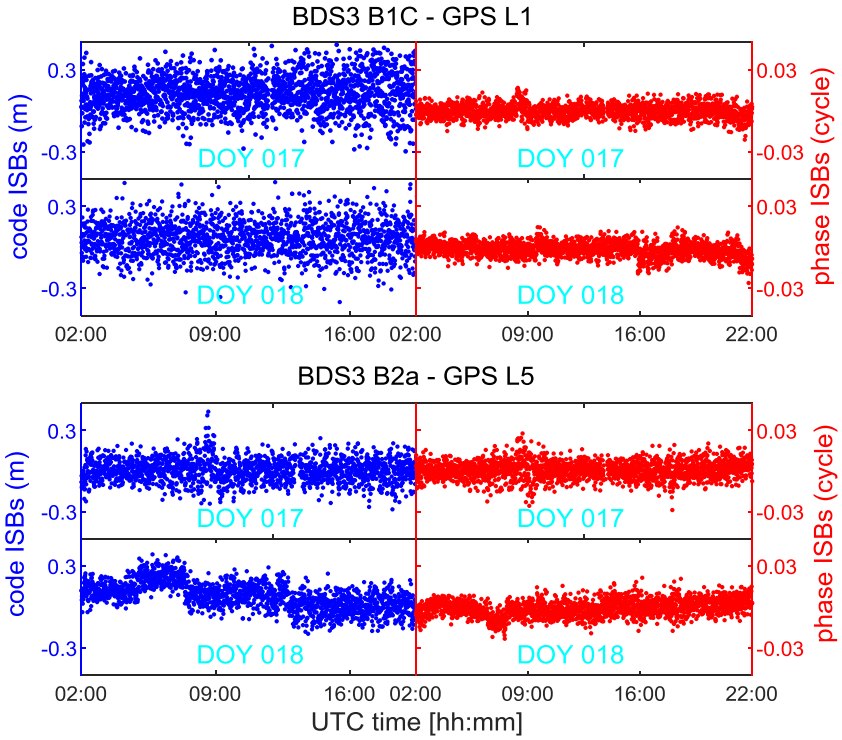

Figure 2. Estimated B1C-L1 and B2a-L5 code (left) and phase (right) ISBs for zero-baseline IGG50-IGG52 on two days (017 and 018 of 2019).

Table 3. Mean and standard deviation of the BDS3-GPS ISBs estimation errors of zero-baseline IGG50-IGG52 and short-baseline IGG50-IGG51.

		Code ISBs (m)				Phase ISBs (cycle)			
		B1C-E1		B2a-E5a		B1C-E1		B2a-E5a	
Baseline	Day	Mean	std	Mean	std	Mean	std	Mean	std
IGG50-IGG52	017	0.11	0.15	0.01	0.03	0.00	0.15	0.00	0.01
	018	0.06	0.14	0.05	0.04	−0.00	0.14	−0.00	0.01
IGG50-IGG51	017	−0.02	0.28	−0.01	0.25	0.02	0.06	−0.00	0.04
	018	0.10	0.40	0.14	0.33	0.01	0.03	−0.02	0.03

The number of satellites visible over 24 h for an elevation cut-off angle of 5° and station IGG52 is given in figure 1, which shows that the number of BDS3 satellites available is small.

The broadcast ephemeris is used to calculate the positions of the satellites, and elevation weighting is used to determine the weights of the observations. In addition, the detection, identification and adaptation (DIA) procedure is used to eliminate outliers (Teunissen 2018, Zaminpardaz and Teunissen 2019), and the integer ambiguity issue is solved by LAMBDA, which can optimize the search efficiency and maximize the success rate (Teunissen 1995).

Results of ISBs estimation

In this section, the estimated code and phase ISBs are applied to the overlapping frequencies between BDS3, GPS and Galileo. In addition, the overlapping and non-overlapping frequencies of ISBs between BDS3 and BDS2 are also investigated. For the sake of brevity, only the results of ISBs estimates for some days during the experiment are reported, which are representative of all the experimental results that we obtained.

ISBs between BDS3 and GPS. The top of figure 2 shows the epoch-by-epoch estimates of B1C-L1 ISBs for zero-baseline IGG50-IGG52 and for two days (017 and 018 of 2019) and the bottom of figure 2 illustrates those of the B2a-L5 ISBs. Focusing on each panel, we see that these estimates fluctuate randomly around zero, with no apparent trend over time. The mean and standard deviation of the ISBs estimation errors of zero-baseline IGG50-IGG52 for both the code and phase ISBs and for all configurations are shown in table 3.

Combining the figures and table above, an important conclusion can be drawn. That is, considering the measurement noise, which is at the level of a few millimeters for the phase ISBs and a few decimeters for the code ISBs, the estimated ISBs both the code and phase ISBs estimates can be regarded as zero. In other words, there is no reason to

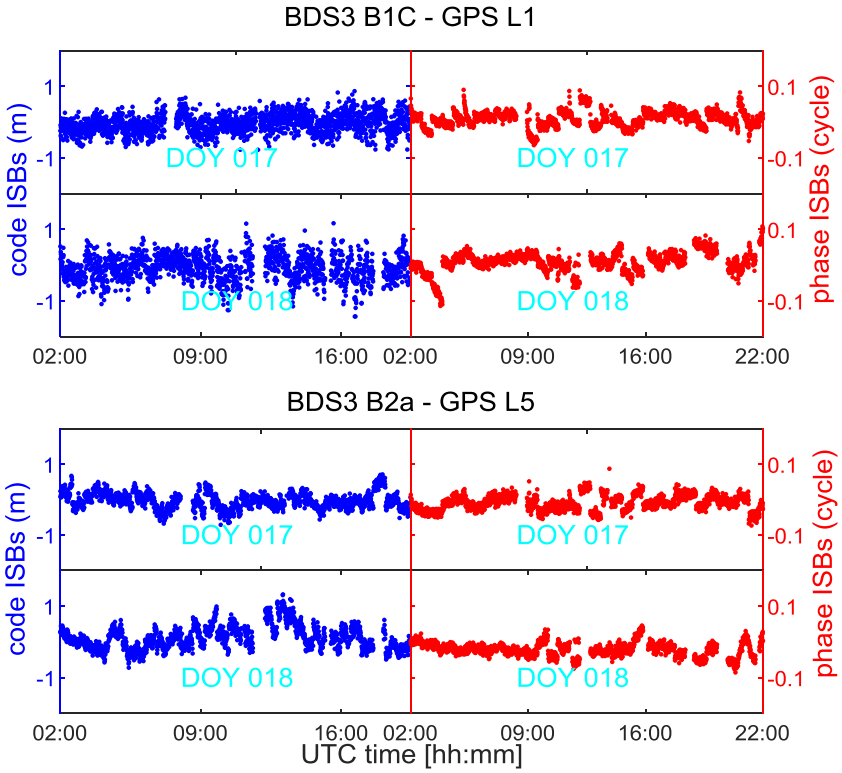

Figure 3. Estimated B1C-L1 and B2a-L5 code (left) and phase (right) ISBs for the short-baseline IGG50-IGG51 on two days (017 and 018 of 2019).

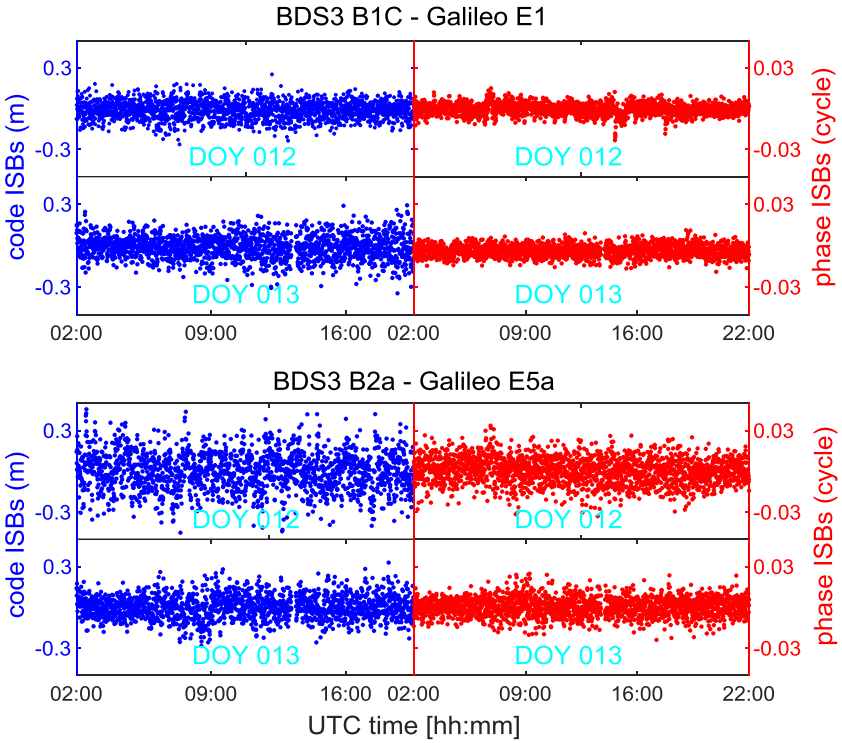

Figure 4. Estimated B1C-E1 and B2a-E5a code (left) and phase (right) ISBs for zero-baseline IGG50-IGG52 on two days (012 and 013 of 2019).

expect ISBs to be present for baselines consisting of identical receiver types; hence, they do not have to be considered when combining the overlapping frequencies of BDS3 and GPS.

Figure 3 shows the estimated phase and code ISBs for B1C-L1 and B2a-L5 of short-baseline IGG50-IGG51, of which the baseline length is 69 m. Unlike the ISBs estimates with zero-baseline IGG50-IGG52, although those estimates

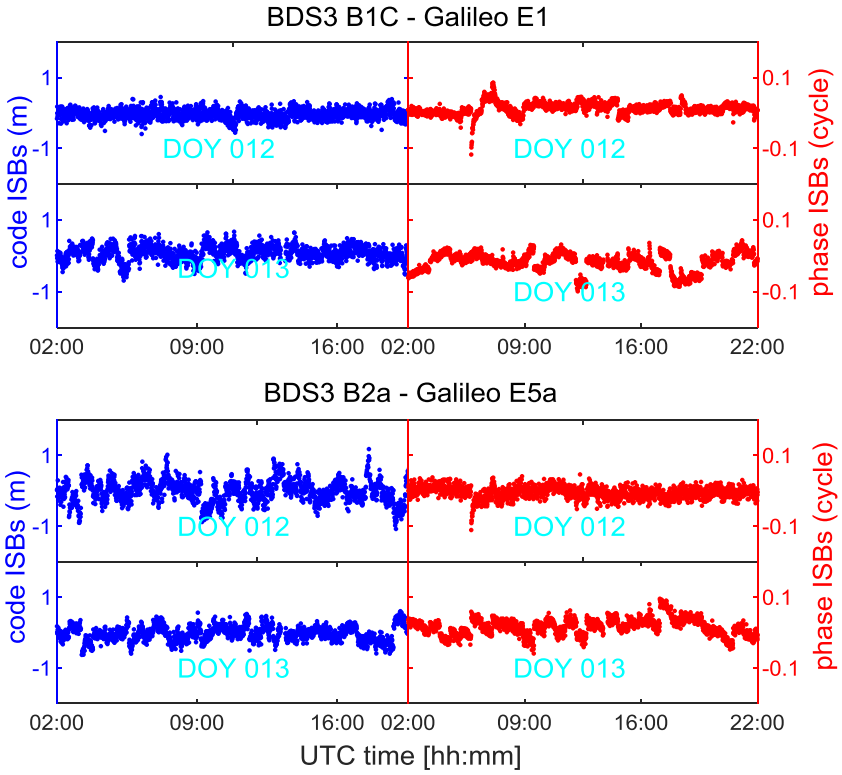

Figure 5. Estimated B1C-E1 and B2a-E5a code (left) and phase (right) ISBs for the short-baseline IGG50-IGG51 on two days (012 and 013 of 2019).

Table 4. Mean and standard deviation of the BDS3-Galileo ISBs estimation errors of zero-baseline IGG50-IGG52 and short-baseline IGG50-IGG51.

		Code ISBs (m)				Phase ISBs (cycle)			
		B1C-E1		B2a-E5a		B1C-E1		B2a-E5a	
Baseline	Day	Mean	std	Mean	std	Mean	std	Mean	std
IGG50-IGG52	012	−0.01	0.07	0.01	0.14	0.00	0.00	0.00	0.01
	013	−0.01	0.10	0.00	0.08	−0.00	0.00	0.00	0.01
IGG50-IGG51	012	−0.04	0.15	−0.02	0.31	0.01	0.02	−0.01	0.01
	013	0.03	0.21	0.01	0.24	−0.01	0.03	0.01	0.02

fluctuated around zero, the estimates are nonstationary and the noise level increases in this case due to the multipath effect. The mean and standard deviation of the code and phase ISBs estimation errors for short-baseline IGG50-IGG51 are also shown in table 3. Based on the data in the table, we can see that although the noise level of the ISBs estimates in this case is larger than that for the zero baseline, the estimates still fall safely within the noise range of the observations. According to the analysis of ISBs between BDS3 and GPS based on both the zero and short baselines, an important conclusion can be drawn: interoperability can be achieved for the overlapping frequencies of BDS3 and GPS.

ISBs between BDS3 and Galileo. Figures 4 and 5 show the B1C-E1 and B2a-E5a ISBs for two baselines and for two days (012 and 013 of 2019). We can see that the estimated BDS3-Galileo ISBs for the zero baseline are randomly distributed around zero and those for the short baseline are not due to multipath effects. Table 4 shows the mean and standard deviation of the BDS3-Galileo ISBs estimation errors for the two baselines. According to the figures and table of the ISBs estimation involving BDS3 and Galileo, we see that interoperability can be achieved not only for the overlapping frequencies of BDS3 and GPS but also for BDS3 and Galileo.

ISBs between BDS3 and BDS2. BDS3 inherits the two frequencies of BDS2 (B1I and B3I) and adds two new frequencies (B1C and B2a), and it is important to determine whether there are ISBs between BDS3 and BDS2 to achieve the transition from BDS2 to BDS3. Figures 6 and 7 show the ISBs of overlapping frequencies B1I and B3I between BDS3 and BDS2 for two baselines on two days (014 and 016 of 2019). The mean and standard deviation of the BDS3-BDS2 overlapping frequency ISBs estimation errors are shown in table 5. The results obtained show that both the zero and short baselines formed with the same receivers are characterized by close to zero code ISBs and zero phase ISBs. Thus, the

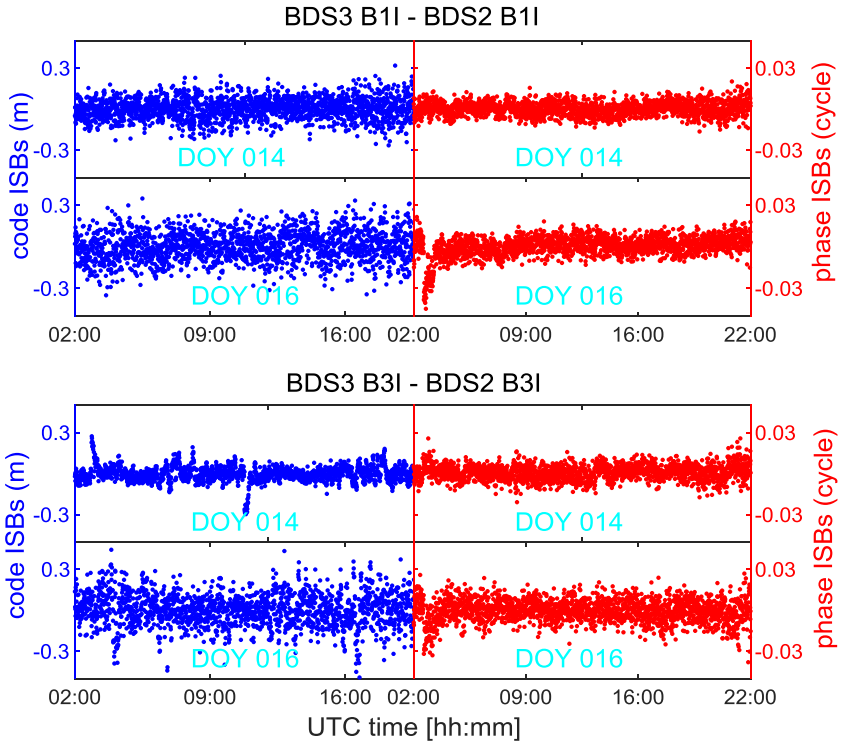

Figure 6. Estimated B1I and B3I code (left) and phase (right) ISBs between BDS3 and BDS2 for the zero-baseline IGG50-IGG52 on two days (014 and 016 of 2019).

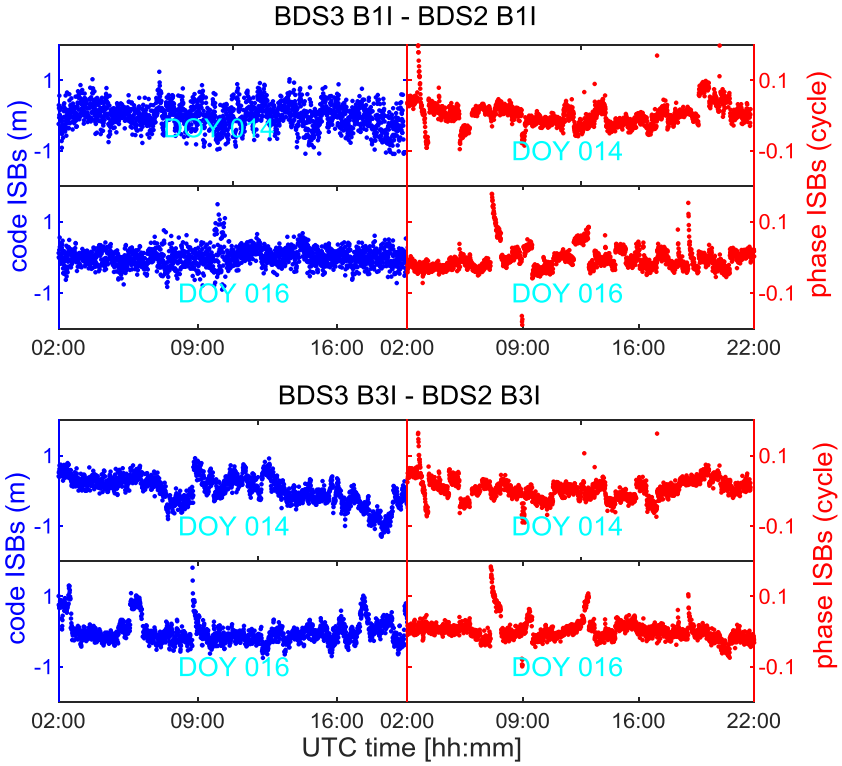

Figure 7. Estimated B1I and B3I code (left) and phase (right) ISBs between BDS3 and BDS2 for short-baseline IGG50-IGG51 on two days (014 and 016 of 2019).

overlapping frequencies of BDS3 and BDS2 can be combined without considering ISBs.

To combine BDS3 with other GNSSs while using the existing BDS2 information, it is advisable to combine the non-overlapping frequencies of BDS3 and BDS2. We have demonstrated that the interoperability of the overlapping frequencies of BDS3 and BDS2 and thus the non-overlapping frequency ISBs between BDS3 and BDS2 are actually differential

Table 5. Mean and standard deviation of the BDS3-BDS2 overlapping frequencies for the B1I and B3I ISBs estimation errors of zero-baseline IGG50-IGG52 and short-baseline IGG50-IGG51 on 014 and 016 in 2019.

		Code ISBs (m)				Phase ISBs (cycle)			
		B1I		B3I		B1I		B3I	
Baseline	Day	Mean	std	Mean	std	Mean	std	Mean	std
IGG50-IGG52	014	−0.01	0.06	0.02	0.12	0.00	0.00	0.00	0.00
	016	0.02	0.09	0.01	0.10	0.01	0.01	0.01	0.01
IGG50-IGG51	014	−0.02	0.19	−0.01	0.21	0.00	0.03	−0.01	0.02
	016	0.01	0.22	0.01	0.23	−0.00	0.03	0.00	0.02

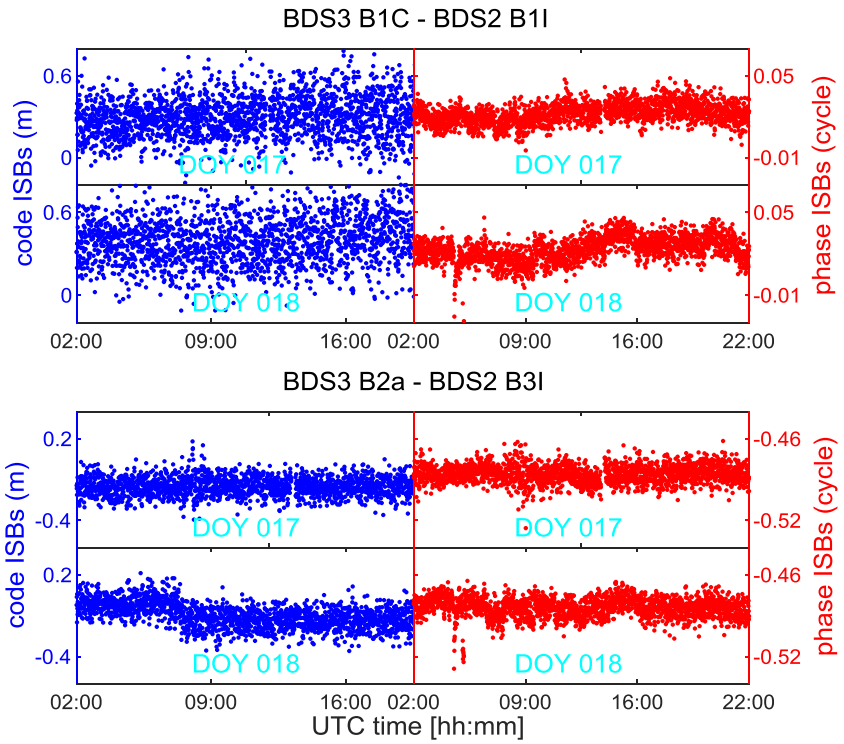

Figure 8. Estimated B1C-B1I and B2a-B3I code (left) and phase (right) ISBs for zero-baseline IGG50-IGG52 on two days (017 and 018 of 2019).

code biases (DCBs) and differential phase biases (DPBs) of the BDS. Figures 8 and 9 show the estimated B1C-B1I and B2a-B3I ISBs between BDS3 and BDS2 for zero-baseline IGG50-IGG52 and short-baseline IGG50-IGG51 on two days (017 and 018 of 2019). Unlike the overlapping frequency ISBs between BDS3 and BDS2, the estimated code and phase ISBs are significant. As shown in table 6, for the zero-baseline case, both the phase and code ISBs are stable, and for the short-baseline case, the ISBs are relatively unstable. The instability of the ISBs estimates for the short-baseline case is due to multipath effects, which is not to say that the ISBs are unstable. The stability of the ISBs suggests that they can be introduced as time-invariant unknowns to improve the RTK positioning performance.

Results of RTK positioning by applying the ISBs

As previously emphasized, the significance of calibrating ISBs lies not in analyzing the ISBs themselves but in improving the performance of multi-GNSS ambiguity resolution and the RTK positioning accuracy. To evaluate the performance of multi-GNSS RTK positioning with ISBs applied, we performed tests with zero-baseline IGG50-IGG52 and short-baseline IGG50-IGG51 on January 12 and 13, 2019. Data were recorded for the new-generation BDS3, BDS2, GPS and Galileo, but we used only dual-frequency observations from each constellation. The frequencies used for each constellation are given in table 7. The RTK model of inter-system differencing in equation (5) is used. Note that the same frequencies are used by BDS3, GPS and Galileo and that there are no ISBs between them has been proved, so we directly set their ISBs to zero as known values. However, the non-overlapping frequency ISBs between BDS3 and BDS2 are very significant, and they are estimated as time-invariant parameters to improve the model strength. To minimize multipath effects, a cut-off elevation of 15° is adopted.

Table 8 presents the ambiguity resolution results in terms of the empirical success rates on 012 and 013 in 2019 and for both zero and short baselines, starting with BDS3 only and then sequentially adding the other constellations.

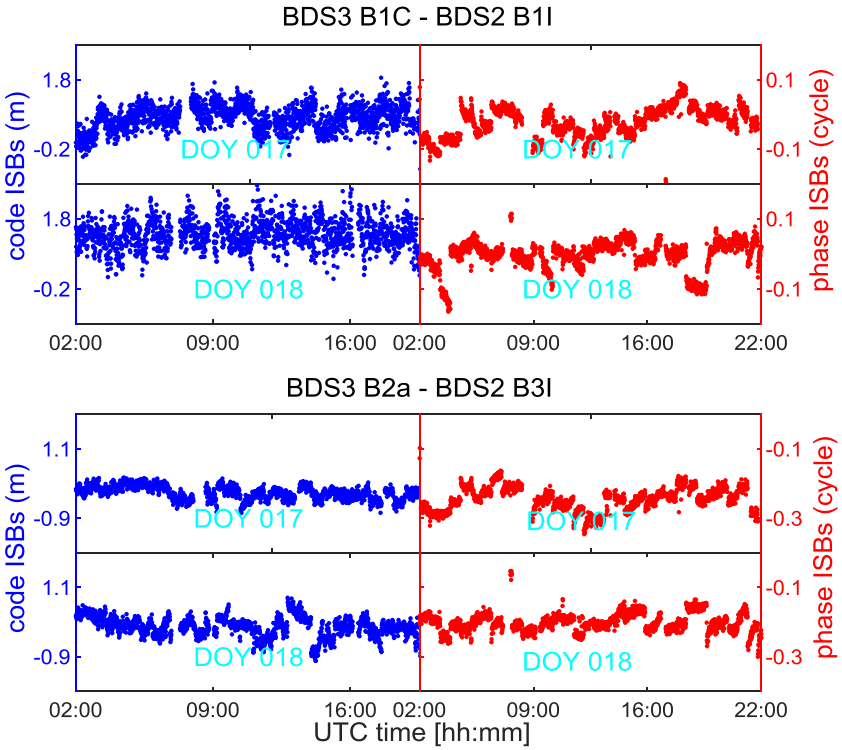

Figure 9. Estimated B1C-B1I and B2a-B3I code (left) and phase (right) ISBs for short-baseline IGG50-IGG51 on two days (017 and 018 of 2019).

Table 6. Mean and standard deviation of the BDS3-BDS2 non-overlapping frequency ISBs estimation errors of zero-baseline IGG50-IGG52 and short-baseline IGG50-IGG51 on 017 and 018 in 2019.

		Code ISBs (m)				Phase ISBs (cycle)			
		B1I		B3I		B1I		B3I	
Baseline	Day	Mean	std	Mean	std	Mean	std	Mean	std
IGG50-IGG52	017	0.29	0.16	−0.03	0.07	0.02	0.01	−0.48	0.01
	018	0.40	0.18	0.02	0.09	0.01	0.01	−0.50	0.01
IGG50-IGG51	017	0.66	0.22	−0.17	0.20	0.03	0.24	−0.20	0.21
	018	0.89	0.24	−0.01	0.29	0.01	0.04	−0.21	0.03

We take the results for zero-baseline IGG50-IGG51 on day 012 of 2019 as an example. First, we focus on BDS3, and epochs with the correct ambiguities resolved are 11.1% of during the day. This poor performance is particularly due to having 4 or less BDS3 satellites available for most of the day. With GPS added, the empirical ambiguity resolution success rate increases significantly to 42.5% for classical differencing compared with 66.9% for inter-system differencing, which represents an improvement of 57.4%. However, because only some GPS satellites modulate the L5 signal, the availability of data is still limited. Due to the accelerated globalization of Galileo and the increasing number of satellites available, adding Galileo data to BDS3 + GPS results in a success rate of 72.0% for classical differencing and 93.0% for inter-system differencing, an increase of 29.2%. The best results are obtained when BDS2 satellites are added to BDS3 + GPS + Galileo, and the success rate is 100% for inter-system differencing, which means that for all epochs during the day, the ambiguities are correctly resolved. The same conclusion can be drawn from the results on 013 and for short-baseline IGG50-IGG51 on both days.

Table 7. Overview of the frequencies used for each GNSS constellation (BDS3, BDS2, GPS and Galileo).

GNSS constellation	Frequencies
BDS3	B1C and B2a
BDS2	B1I and B3I
GPS	L1 and L5
Galileo	E1 and E5a

Figures 10 and 11 show the positioning results for four different combinations (BDS3, BDS3 + GPS, BDS3 + GPS + Galileo and BDS3 + GPS + Galileo + BDS2) of IGG50-IGG52 on days 012 and 013 of 2019, where the horizontal position scatter and the vertical position time series are available. We can see that the

Table 8. Empirical integer ambiguity resolution success rates for zero-baseline IGG50-IGG52 and short-baseline IGG50-IGG51 based on dual-frequency data on days 012 and 013 (**bold**) of 2019.

	IGG50-IGG52		IGG50-IGG51	
	Classical	Inter-system	Classical	Inter-system
BDS3	11.1%	—	4.4%	—
	15.9%	—	**11.0%**	—
BDS3 + GPS	42.5%	66.9%	35.9%	57.7%
	40.7%	**77.3%**	**44.3%**	**74.0%**
BDS3 + GPS + Galileo	72.0%	93.0%	68.9%	95.2%
	70.8%	**97.2%**	**66.8%**	**95.9%**
BDS3 + GPS + Galileo + BDS2	96.8%	100%	95.5%	99.9%
	95.2%	**100%**	**96.4%**	**99.6%**

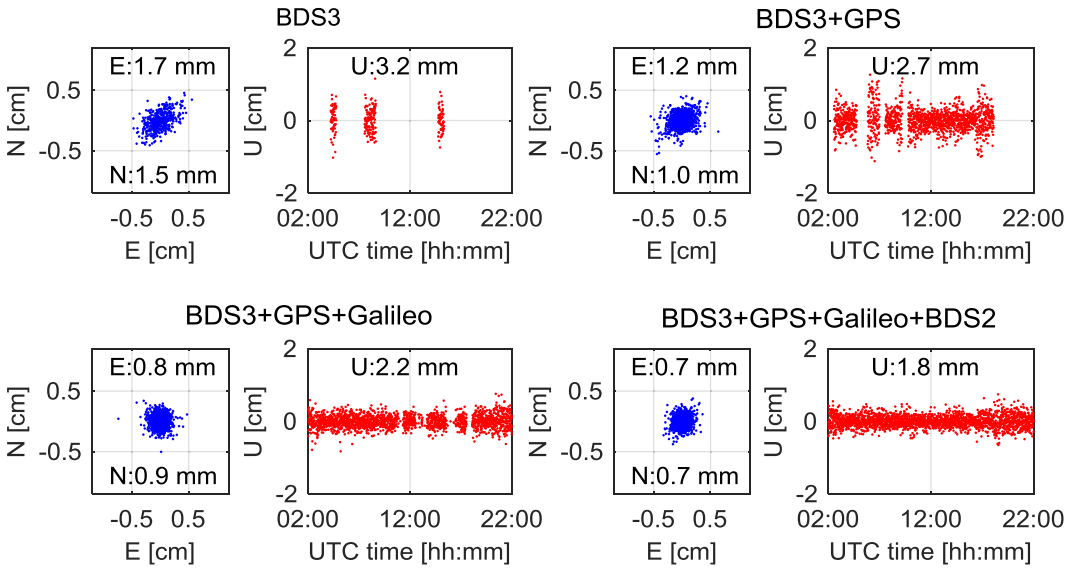

Figure 10. Horizontal (E = East and N = North) position scatter and vertical (U = Up) time series based on inter-system differencing for zero-baseline IGG50-IGG52 on day 012 of 2019 for BDS3 (top left), BDS3 + GPS (top right), BDS3 + GPS + Galileo (bottom left) and BDS3 + GPS + Galileo + BDS2 (bottom right).

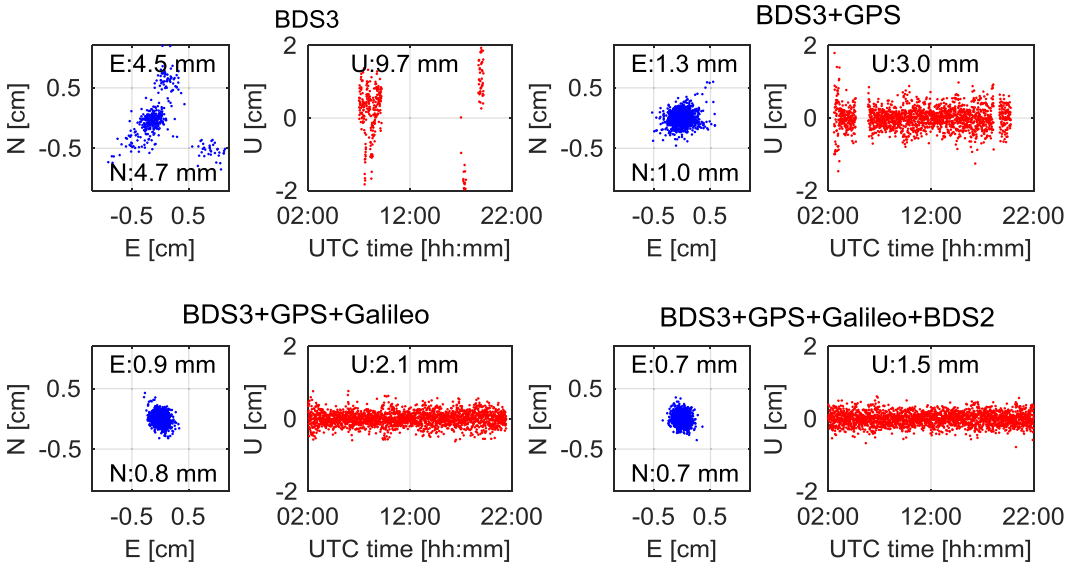

Figure 11. Horizontal (E = East and N = North) position scatter and vertical (U = Up) time series based on inter-system differencing for zero-baseline IGG50-IGG52 on day 013 of 2019 for BDS3 (top left), BDS3 + GPS (top right), BDS3 + GPS + Galileo (bottom left) and BDS3 + GPS + Galileo + BDS2 (bottom right).

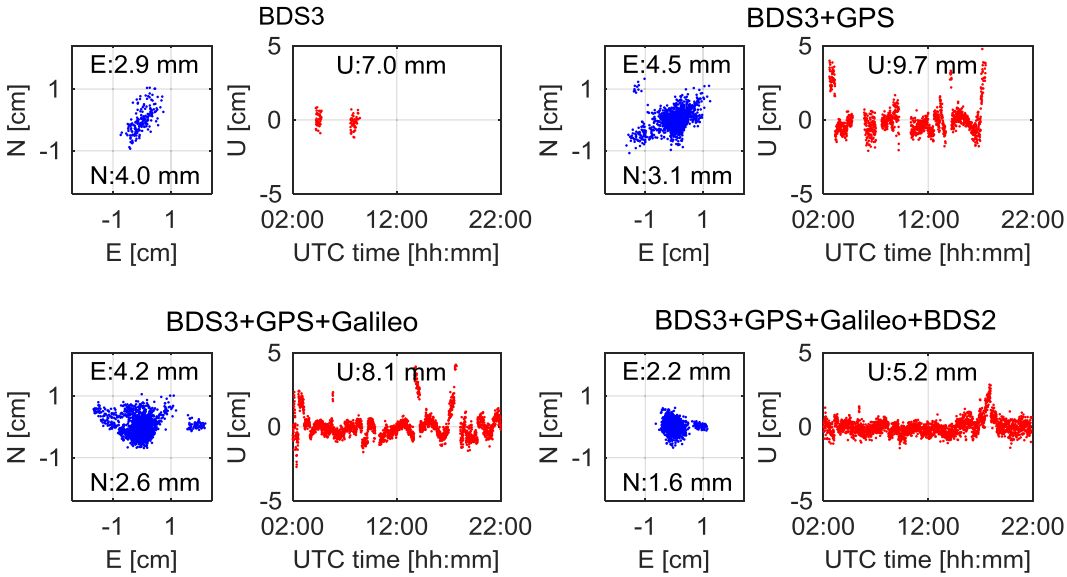

Figure 12. Horizontal (E = East and N = North) position scatter and vertical (U = Up) time series based on inter-system differencing for short-baseline IGG50-IGG51 on day 012 of 2019 for BDS3 (top left), BDS3 + GPS (top right), BDS3 + GPS + Galileo (bottom left) and BDS3 + GPS + Galileo + BDS2 (bottom right).

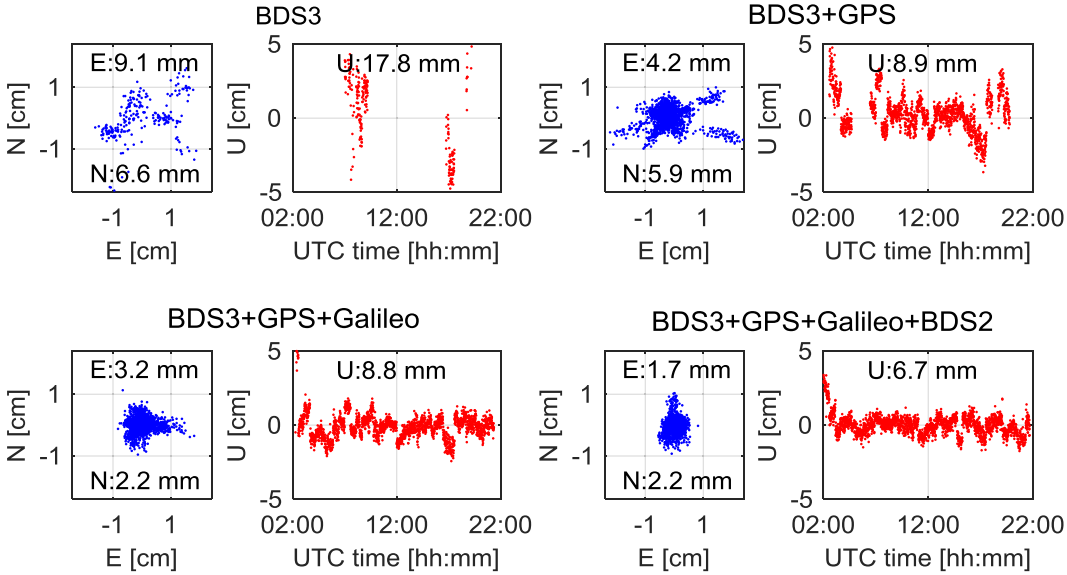

Figure 13. Horizontal (E = East and N = North) position scatter and vertical (U = Up) time series based on inter-system differencing for short-baseline IGG50-IGG51 on day 013 of 2019 for BDS3 (top left), BDS3 + GPS (top right), BDS3 + GPS + Galileo (bottom left) and BDS3 + GPS + Galileo + BDS2 (bottom right).

availability of the positioning solutions of new-generation BDS3 is low, which suggests that BDS3 cannot currently provide positioning information 24h per day independently. However, the availability of the positioning solutions clearly increases when going from one to multiple constellations, as shown in both graphs, which reflects higher availability and positioning accuracy in complex environments using the inter-system differencing with multi-GNSS constellations compared to the results of traditional methods. In addition, the root mean square (RMS) values of three directions are shown in each graph. These results clearly illustrate the improvements in the positioning accuracy when going from one to multiple constellations. Figures 12 and 13 show that the results are analogous to those in figures 10 and 11, except for short-baseline IGG50-IGG51, and the multipath effect is significant.

Conclusion

The new-generation BDS3 has started to provide basic services, and its compatibility and interoperability with other GNSSs are of great concern to global users. In this study, we extended our proposed SD method for determining the ISBs of BDS3 satellites. The main contribution of this work consists in that the ISBs between BDS3, GPS, Galileo and BDS2 and the RTK performance of inter-system differencing based on BDS3 were analyzed for the first time.

We have demonstrated that for the overlapping frequencies of BDS3, GPS and Galileo, there is no reason to expect ISBs to be present, which suggests that interoperability can be achieved between these three constellations. However, the

ISBs of BDS3 and BDS2 are significant for non-overlapping frequencies but not for overlapping frequencies. When mixing the overlapping and non-overlapping frequencies of BDS3 and BDS2, the ISBs must be considered. Furthermore, the integer ambiguity resolution success rates of inter-system differencing are improved by 25%–60% compared with those of classical differencing, and this approach considerably benefits multi-GNSS RTK positioning in difficult environments.

Acknowledgments

This work was partially funded by the National Natural Science Foundation of China (Grant Nos. 41604031, 41774042, and 41621091) and the National Key Research Program of China Collaborative Precision Positioning Project (Grant No. 2016YFB0501900). The second author is supported by the CAS Pioneer Hundred Talents Program. The third author acknowledges the LU JIAXI International team program supported by the KC Wong Education Foundation and CAS.

ORCID iDs

Xiaolong Mi https://orcid.org/0000-0003-2950-3472
Baocheng Zhang https://orcid.org/0000-0001-5006-1432

References

Cao Y *et al* 2019 Initial analysis of the BDS satellite autonomous integrity monitoring capability *GPS Solut.* **23** 25
Deng C, Tang W, Liu J and Shi C 2014 Reliable single-epoch ambiguity resolution for short baselines using combined GPS/BeiDou system *GPS Solut.* **18** 375–86
El-Mowafy A, Deo M and Rizos C 2016 On biases in precise point positioning with multi-constellation and multi-frequency GNSS data *Meas. Sci. Technol.* **27** 035102
Gao W, Gao C, Pan S, Meng X and Xia Y 2017 Inter-system differencing between GPS and BDS for medium-baseline RTK positioning *Remote Sens.* **9** 948
Gao W, Pan S, Gao C, Wang Q and Shang R 2019 Tightly combined GPS and GLONASS for RTK positioning with consideration of differential inter-system phase bias *Meas. Sci. Technol.* **30** 054001
Gioia C and Borio D 2016 A statistical characterization of the Galileo-to-GPS inter-system bias *J. Geod.* **90** 1279–91
Jiang N, Xu Y, Xu T, Xu G, Sun Z and Schuh H 2017 GPS/BDS short-term ISB modelling and prediction *GPS Solut.* **21** 163–75
Li G, Wu J, Zhao C and Tian Y 2017 Double differencing within GNSS constellations *GPS Solut.* **21** 1161–77
Li X, Xie W, Huang J, Ma T, Zhang X and Yuan Y 2019 Estimation and analysis of differential code biases for BDS3/BDS2 using iGMAS and MGEX observations *J. Geod.* **93** 419–35
Liu J, Tu R, Han J, Zhang R, Zhang P, Fan L and Lu X 2019 Inter-system biases in GPS and BDS combined relative positioning by double-differenced observations *Meas. Sci. Technol.* **30** 085001
Mi X, Zhang B and Yuan Y 2019a Stochastic modeling of between-receiver single-differenced ionospheric delays and its application to medium baseline RTK positioning *Meas. Sci. Technol.* **30** 095008
Mi X, Zhang B and Yuan Y 2019b Multi-GNSS inter-system biases: estimability analysis and impact on RTK positioning *GPS Solut.* **23** 81
Nadarajah N, Teunissen P J G, Sleewaegen J-M and Montenbruck O 2014 The mixed-receiver BeiDou inter-satellite-type bias and its impact on RTK positioning *GPS Solut.* **19** 357–68
Odijk D and Teunissen P J G 2010 Improving the speed of CORS Network RTK ambiguity resolution *Proc. IEEE/ION PLANS 2010 (Indian Wells, CA, 4–6 May)* pp 79–84
Odijk D and Teunissen P J G 2012 Characterization of between-receiver GPS-Galileo inter-system biases and their effect on mixed ambiguity resolution *GPS Solut.* **17** 521–33
Odijk D, Nadarajah N, Zaminpardaz S and Teunissen P J G 2016 GPS, Galileo, QZSS and IRNSS differential ISBs: estimation and application *GPS Solut.* **21** 439–50
Odolinski R, Odijk D and Teunissen P J G 2014a Combined GPS and BeiDou instantaneous RTK positioning *J. Inst. Navig.* **61** 135–48
Odolinski R, Teunissen P J G and Odijk D 2013 Quality analysis of a combined COMPASS/BeiDou-2 and GPS RTK positioning model *Methodology* **5** 25–48
Odolinski R, Teunissen P J G and Odijk D 2014b Combined BDS, Galileo, QZSS and GPS single-frequency RTK *GPS Solut.* **19** 151–63
Odolinski R, Teunissen P J G and Odijk D 2014c First combined COMPASS/BeiDou-2 and GPS positioning results in Australia. Part II: single- and multiple-frequency single-baseline RTK positioning *J. Spat. Sci.* **59** 25–46
Odolinski R, Teunissen P J G and Odijk D 2015 Combined GPS + BDS for short to long baseline RTK positioning *Meas. Sci. Technol.* **26** 045801
Paziewski J and Wielgosz P 2014 Accounting for Galileo–GPS inter-system biases in precise satellite positioning *J. Geod.* **89** 81–93
Paziewski J, Sieradzki R and Wielgosz P 2015 Selected properties of GPS and Galileo-IOV receiver intersystem biases in multi-GNSS data processing *Meas. Sci. Technol.* **26** 095008
Teunissen P J G 1995 The least-squares ambiguity decorrelation adjustment: A method for fast GPS integer ambiguity estimation *J. Geod.* **70** 65–82
Teunissen P J G 2018 Distributional theory for the DIA method *J. Geod.* **92** 59–80
Wang M, Wang J, Dong D, Meng L, Chen J, Wang A and Cui H 2019 Performance of BDS-3: satellite visibility and dilution of precision *GPS Solut.* **23** 56
Yang Y *et al* 2014 Preliminary assessment of the navigation and positioning performance of BeiDou regional navigation satellite system *Sci. China Earth Sci.* **57** 144–52
Yang Y, Gao W, Guo S, Mao Y and Yang Y 2019 Introduction to BeiDou-3 navigation satellite system *Navigation* **66** 7–18
Yang Y, Xu Y, Li J and Yang C 2018 Progress and performance evaluation of BeiDou global navigation satellite system: data analysis based on BDS-3 demonstration system *Sci. China Earth Sci.* **61** 614–24
Zaminpardaz S and Teunissen P J G 2019 DIA-datasnooping and identifiability *J. Geod.* **93** 85–101
Zhang B, Teunissen P J G and Yuan Y 2016 On the short-term temporal variations of GNSS receiver differential phase biases *J. Geod.* **91** 563–72
Zhang X, Wu M, Liu W, Li X, Yu S, Lu C and Wickert J 2017 Initial assessment of the COMPASS/BeiDou-3: new-generation navigation signals *J. Geod.* **91** 1225–40
Zhao Q, Wang C, Guo J, Wang B and Liu J 2017 Precise orbit and clock determination for BeiDou-3 experimental satellites with yaw attitude analysis *GPS Solut.* **22** 4